Effect of Mesoscale Ordering on the Density of States of Polymeric Semiconductors

Patrick Gemünden, Carl Poelking, Kurt Kremer,* Kostas Daoulas,* Denis Andrienko*

A multiscale simulation scheme, which incorporates both long-range conformational disorder and local molecular ordering, is proposed for predicting large-scale morphologies and charge transport properties of polymeric semiconductors. Using poly(3-hexylthiophene) as an example, it is illustrated how the energy landscape and its spatial correlations evolve with increasing degree of structural order in mesophases with amorphous, uniaxial, and biaxial nematic ordering. It is shown that the formation of low-lying energy states in more ordered systems is mostly due to larger (on average) conjugation lengths and not due to electrostatic interactions. The proposed scheme is general and can be applied to a wide range of polymeric organic materials.

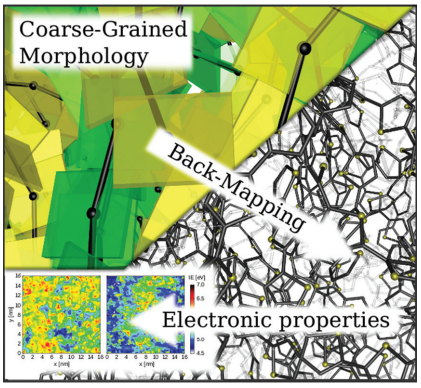

1. Introduction

Solution processing and mechanical flexibility are two features that render polymeric semiconductors promising materials for organic electronic devices, including field-effect transistors, solar cells, or light-emitting diodes. In order to control solubility and self-assembly of polymeric semiconductors, the polymer conjugated backbone is often decorated with, e.g., alkyl side chains, which prevent chain aggregation and promote their lamellar packing, thus facilitating charge transport.[1,2] Furthermore, by changing side-chain and backbone architectures, as well as side-chain length and attachment density, one can in principle adjust both morphological and electronic properties of the polymer and tailor its properties (charge mobility, light absorption, electronic level alignment) for a specific application. The aim of computer simulations is to assist with the design by (i) predicting molecular ordering (including defects) in large-scale morphologies and (ii) elucidating the effect of morphology on electronic processes, in particular charge transport.[3–8]

Let us first address the issue of morphology prediction. The target here is to devise an algorithm which takes chemical structures and processing conditions as an input and generates nanometer-large, atomistically resolved morphologies. Taking into account the required (atomistic) resolution, atomistic molecular dynamics (MD) with an appropriately parametrized force field seems to be the method of choice.[5,9–11] MD, however, is computationally demanding: simulation times are limited to microseconds, which is insufficient to observe polymer self-assembly. In order to speed up molecular dynamics,

P. Gemünden, C. Poelking, Prof. K. Kremer, Dr. K. Daoulas, Dr. D. Andrienko
Max Planck Institute for Polymer Research, 55128 Mainz, Germany
E-mail: kremer@mpip-mainz.mpg.de; daoulas@mpip-mainz.mpg.de; denis.andrienko@mpip-mainz.mpg.de

DOI: 10.1002/marc.201400725

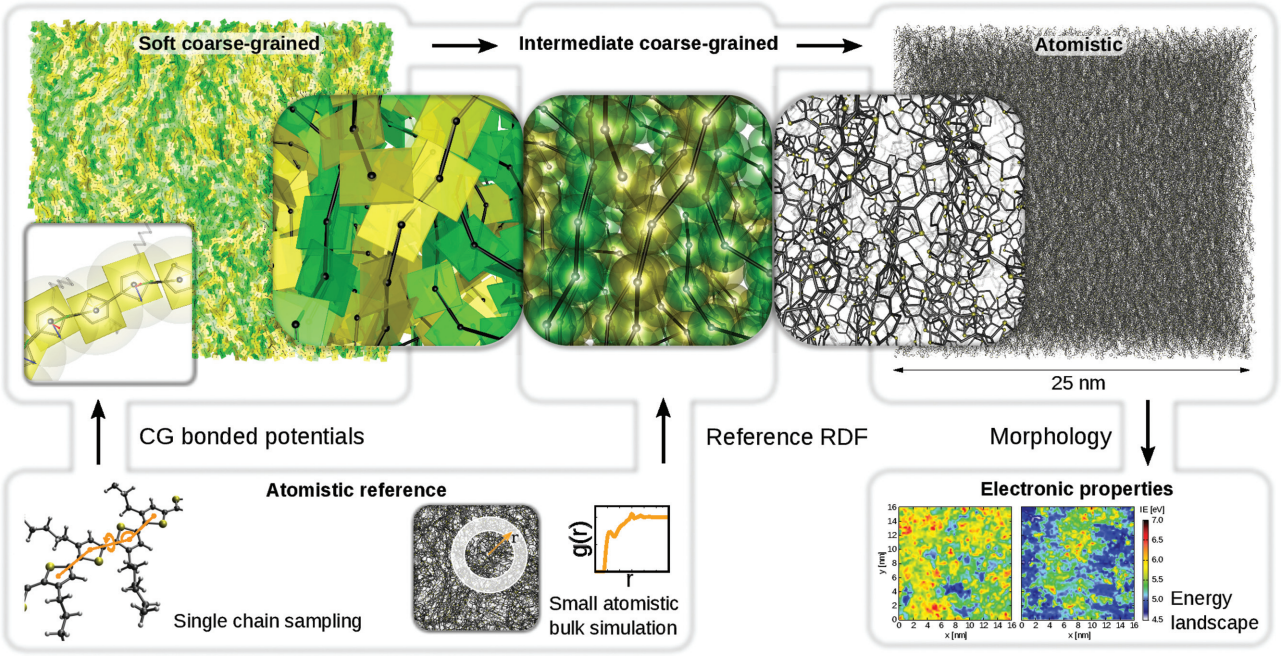

Figure 1. Strategy for generating large-scale morphologies of conjugated polymers. To obtain a low-resolution description, entire repeat units are coarse-grained into soft particles with plate-like symmetry (top left panel, shown with two colors for better visibility), with the bonded potentials parametrized on sampling of a single chain (bottom left). Subsequently, overlaps are removed using an intermediate model (top middle panel) obtained by structure-based coarse-graining of an all-atom polymer melt with a single-bead representation of each repeat unit, including the side chain (bottom middle). Eventually, all atoms on backbones and side chains are re-introduced and the local molecular packing is relaxed (top right panel). The atomistic morphology obtained from this procedure serves as an input for calculations of electronic properties (bottom right).

coarse-grained (CG) models are often employed.[12–16] Softer interaction potentials of CG models[17] result in a reduction of friction forces, larger simulation time-steps, and hence more efficient sampling of the phase space. For polymeric systems with their slow dynamics, a significant reduction of the number of degrees of freedom is normally required, with entire monomers represented by single interaction sites.

As a drawback of drastic coarse-graining, CG models can either be tuned to thermodynamic or structural properties. In our particular case, the CG model yields correct large-scale polymer chain statistics, but compromises local molecular packing (often leading to chain overlaps), complicating the reintroduction of atomistic details into a coarse-grained morphology (backmapping). This is the first issue we will address in this paper. Our idea is to introduce an intermediate, structure-based, coarse-grained model capable of adjusting local chain packing without affecting global chain configurations. The intermediate morphologies can then be used to reintroduce atomistic details (see Figure 1).

With large-scale atomistic morphologies at hand, one can further investigate electronic properties of polymeric semiconductors, in particular the charge-carrier mobility. Charge transport is an example of a process affected by morphological features across multiple scales: it is sensitive both to the atomistic structure of the material (via site energetics and electronic couplings) and to the mesoscopic ($\gtrsim$10 nm) polymer alignment, via fast charge-carrier motion along the conjugated backbone.[18,19] Therefore, molecular understanding of transport requires large and at the same time atomistically resolved morphologies. To simulate charge transport in these partially ordered morphologies, there is in principle no alternative to computing the electronic wavefunction of the entire system. Since the excited state of the charged system cannot be computed even with modern quantum-chemical methods, all approaches to evaluate the wavefunction of large systems have focused on neutral polymers and thus interpret one-electron states as charge localization sites.[20] As a result, electron and nuclear polarization effects due to the excess charge have not been taken into account. This is the second issue we would like to address here: using a perturbative scheme, we assess Coulombic and polarization effects on the density of states.

Both approaches are illustrated on poly(3-hexylthiophene) (P3HT), a fruit fly of the organic semiconductor community.[20] Charge transport in P3HT has been studied with the aim of relating polymer regioregularity and molecular weight to the morphology, hole mobility, and thus efficiency of bulk heterojunction solar cells. Both hole and electron time-of-flight mobilities were reported to be

independent of the molecular weight up to 20 kDa, which then decreased by an order of magnitude as molecular weight was further increased to 120 kDa.[21] The field-effect mobility was found to increase with the molecular weight in spite of reduced crystallinity. This was attributed to either better interconnectivity of the polymer network[18] or smaller intrachain ring torsions present in high molecular weight molecules.[22]

2. Results and Discussion

In order to understand the role of chain ordering on charge transport, we have analyzed three types of molecular ordering: amorphous, uniaxial nematic, and biaxial nematic. Large-scale morphologies of these mesophases were generated using the soft-core CG model, with a P3HT repeat unit (thiophene ring and the alkyl side chain) mapped onto a single interaction site. Model details can be found elsewhere.[23] The nonbonded interaction potential in this model is anisotropic: by tuning the strength of the anisotropic interaction one can simulate amorphous, uniaxial, and biaxial molecular arrangements. We will now detail the workflow from Figure 1 that summarizes the steps necessary to arrive at large atomistic models based on this soft-core CG input.

The Monte Carlo reptation algorithm was employed to equilibrate 847 chains (3470 chains for the amorphous test system) of 20 repeat units each in the *NVT* ensemble at $T = 500$ K. With the soft-core CG model, the equilibration of even longer chains is straightforward.[23] Here we study regioregular P3HT only, since we do not expect significant morphological differences for regiorandom chains in the amorphous and nematically ordered phases. As expected, the morphologies obtained using soft potentials lack realistic local packing: segments can even overlap, as can be seen from the radial distribution function (RDF), shown in Figure 2a. It is therefore impossible to directly reinsert the atomistic details of backbones and side chains into the coarse-grained morphology: the local structure is too far off from a realistic chain packing. To remedy the situation, we first adjusted the position of CG beads via an intermediate CG model, derived according to Hendersen's theorem[24] stating that there is a one-to-one correspondence between the pair interaction potential (up to an additive constant) and the radial distribution function. The CG potential of this intermediate CG model results from an iterative Boltzmann inversion[25,26] in a system of 400 regioregular atomistically resolved chains of 20 repeat units each simulated at $T = 500$ K. The atomistic melt was simulated using a tailored force field[10] and the GROMACS package.[27] The Boltzmann inversion was carried out with the VOTCA package,[28] the resulting potential is shown in Figure 2b.

The reintroduction of atomistic details proceeds then as follows. The local molecular packing is first refined by introducing thiophene rings, with ring orientations adjusted to match the orientations of plates in the soft coarse-grained morphology. The nonbonded potentials between the atoms are switched off and the mapping centers interact via the coarse-grained potential derived in the previous step. Subsequently, very short MD runs ensure that chains move by less than one repeat unit. This is especially important for biaxial mesophases, in which collective ordering proves very sensitive to local translations and rotations.

Having recovered the excluded volume per repeat unit, we remove the potential of mean force acting between these units, instead adding atomistic interactions. At this point it is crucial to remove the overlaps of the (so

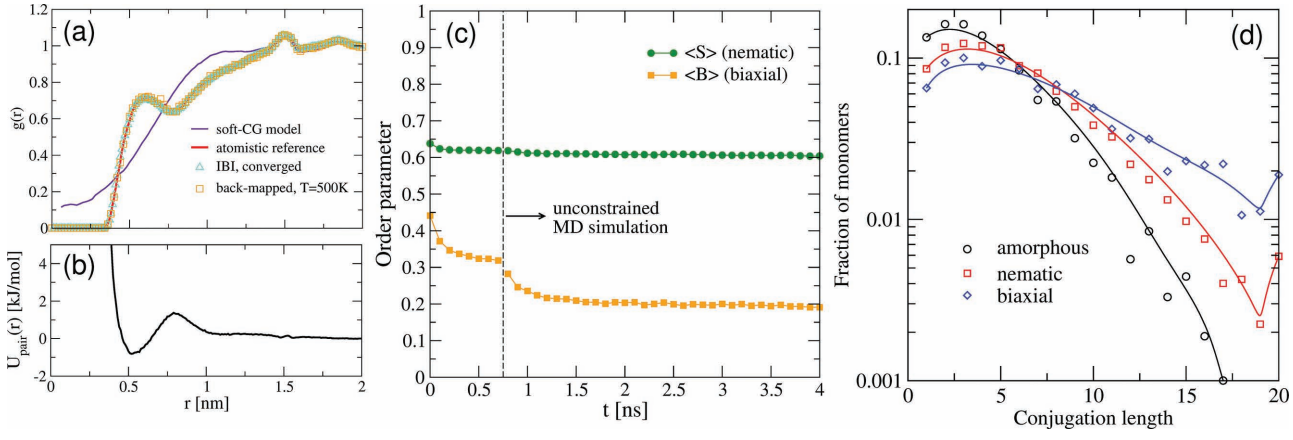

Figure 2. a) Radial distribution functions (RDFs) of thiophene backbones obtained for the soft coarse-grained, IBI-coarse-grained, atomistic, and back-mapped amorphous models. The soft CG model morphologies reproduce atomistic packing on length scales larger than the thiophene–thiophene excluded volume. After the back-mapping step, the local packing is also reproduced. b) Intermediate coarse-grained potential derived using IBI. c) Evolution of the nematic (*S*) and biaxial nematic (*B*) order parameters in a biaxial mesophase during backmapping at $T = 300$ K. d) Fraction of monomers in the system that form part of a conjugated segment of length *l* in the backmapped systems.

far) phantom side-chains with neighboring molecules, while preserving the global morphology. This is achieved by constraining the backbone, here by adding restraints to the positions of the CG mapping centers. At this step, we used stochastic dynamics with force-capped Lennard–Jones (LJ) interactions implemented in the GROMACS package (for details, see the Supporting Information). To allow sufficient time for side-chain relaxation we ensured that the end groups moved by a distance of a few carbon bond-lengths on average. Subsequently, full LJ and Coulomb potentials are switched on. During this stage torsional degrees of freedom in the backbone were restrained in order to prevent reorientations of thiophene rings. All relaxations were performed at T = 500 K to ensure sufficient chain mobility. For the final equilibration, all constraints are removed and MD simulations in the *NPT* ensemble are performed until energy and mass density have stabilized (several nanoseconds). For the amorphous mesophase, the RDF of the back-mapped melt, obtained at T = 500 K and shown in Figure 2a, is in excellent agreement with the RDF of the atomistic reference melt (note that for the other two mesophases, such an atomistic reference is not available). To study electronic properties, we quenched the equilibrated melts to 300 K, with a resulting density of ≈1.03 g cm^{-3} that matches well the experimentally measured value.[29]

For biaxial mesophases the final equilibration is performed directly at T = 300 K, since at higher temperatures (e.g., $T \approx$ 400 K) biaxial ordering becomes unstable upon removing the constraints. Figure 2c shows the evolution of the uniaxial and biaxial nematic order parameters[23] during the equilibration runs. The former measures the degree of collective parallel alignment of the backbones, the latter the degree of collective planar orientation. After removing torsional restraints in the last step of equilibration we observe a slight decrease in the biaxial order, which is due to the relaxation of the dihedral angles in the fully atomistic system. One can see that both order parameters saturate within a few nanoseconds.

We now link molecular conformations and cooperative chain alignment to properties relevant to charge transport.

In partially ordered organic semiconductors charges are typically localized on molecules or their conjugated segments. Within these segments π-conjugation leads to an instantaneous delocalization of a charge carrier, while between the segments π-conjugation is broken. Charge transport proceeds via a series of hopping events, that is, charge transfer reactions, between the conjugated segments. Due to spatial heterogeneity on a microscopic scale, the free energy of the system in the product and adduct states of a single transfer reaction can be different, leading to a spatially inhomogeneous, rugged, energetic landscape and a broadened density of states (DOS). As the hopping rate depends exponentially on the product/adduct free-energy difference, charge mobility is very sensitive to the distribution of site energies, their spatial correlation, and the particular pathway a charge undertakes in a material.[30–32]

Hence, calculation of the energy landscape requires access to both local and nonlocal structure. An atomistic level of resolution allows for the accurate parametrization of molecular fields and field responses. Here we obtain the density of states (DOS) by first partitioning the system onto localization units, and subsequently evaluating the ionization energy for each unit, taking into account electrostatic and inductive contributions that result from the interaction of the hole with the molecular environment. Other approaches include a combination of atomistic molecular dynamics simulations with calculations of electronic structure using tight-binding,[5,33–36] fragment molecular orbital,[37] charge-patching,[38–40] tight-binding DFT,[41,42] as well as semi-empirical approaches.[43,44] More details can be found in ref. [20].

The partitioning onto localization units was performed by imposing a phenomenological criterion for conjugation: If the torsional deviation from planarity between bonded thiophene monomers exceeds ±45°, conjugation between those two monomers is assumed broken.[23] An empirical assessment of this kind has been indicated to fail in some cases,[20,36] but still provides a reasonable approximation to the distribution of conjugation lengths through identification of sufficiently planar segments. Figure 2d reflects this distribution via the fraction of monomers that form part of a conjugated segment of length l. As expected, with increasing ordering from amorphous via nematic to biaxial, the frequency of small conjugation lengths ($l \leq 6$) decreases in favor of larger conjugation lengths ($l > 6$). Additionally, the nematic and biaxial mesophases both exhibit a small jump in frequency toward fully conjugated chains, which in the biaxial case is, however, significantly reduced compared to the initial soft coarse-grained model, in line with the partial loss in biaxial order upon backmapping.

With the systems partitioned onto localization units, we now turn to the resulting energy landscapes. Here we have employed a long-range corrected perturbative treatment in a classical expansion, where molecular electrostatic potentials and the molecular polarizability are parametrized via atom-centered distributed multipoles and polarizabilities, respectively.[45] An account of long-range interactions is desired to capture all effects that accompany nonlocal ordering. Here it is realized by embedding a 3 nm polarization cloud around the charged segment in a periodic prepolarized background that defines the polarization state of the ground-state system. Field interactions are treated in an Ewald-type fashion, while taking into account self-consistent polarization.[6] Additionally,

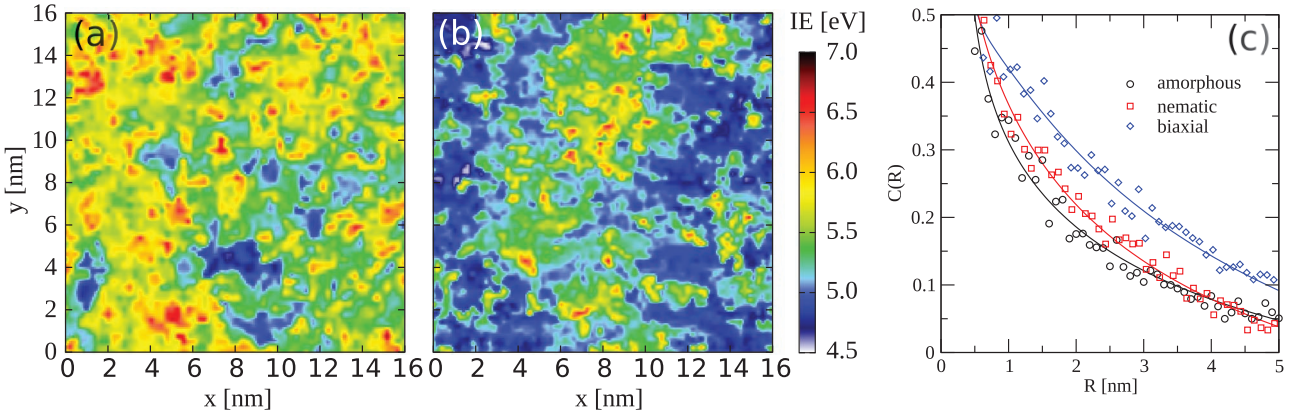

Figure 3. Projection of the ionization energy landscape for holes over a 2 nm-thick slice through the amorphous a) and biaxial b) mesophase. Formation of extended low-IE next to defect-laden regions sets energetics in the biaxial system apart from the amorphous case. In the biaxial case, the nematic director coincides with the *x*-axis. c) Spatial site-energy correlation function for the amorphous, nematic, and biaxial mesophases. The increase of spatial correlations is the combined effect of long-range order—most pronounced for the biaxial system—and electrostatic interactions.

a cube shape-term removes the conditional convergence that can result from the interaction of a charge with a net-quadrupolar environment. Altogether, the ionization energy (IE) is the sum of three terms, the gas-phase ionization energy evaluated for a P3HT chain of length l via density functional theory (B3LYP/6-311g) plus the first-order electrostatic and second-order polarization contributions. Note that this procedure neglects nuclear polarization of the environment. The internal reorganization energy, ranging between 0.2 eV ($l = 1$) to 0.05 eV ($l = 20$) for a planar molecular conformation, should, however, serve as a generous upper limit for this additional stabilization.

Figure 3 shows the projection of the ionization energy landscape over a 2 nm slice of the amorphous and biaxial systems: The amorphous mesophase is characterized by a strongly fragmented energy landscape, whereas the biaxial system, with chains preferentially oriented along the *x*-axis, displays extended low-IE regions that align with the nematic director, next to high-IE islands where defects tend to cluster. These defects are, however, primarily the result of conjugation defects rather than strong fluctuations in molecular fields.

To arrive at a quantitative picture, we disentangle spatial and distributional components by considering the total DOS (Figure 4a) and the spatial correlation function (Figure 3c) individually. We first discuss the former, where we have observed a decrease of the monomer peak at high IE (Figure 4a) and simultaneous extension of the DOS towards lower IEs, with increasing structural order from amorphous via nematic to biaxial. In fact, due to the stronger delocalization of charges in the low-IE region and hence larger volume associated with those states, the change from amorphous to biaxial is more drastic than it may appear from considering the DOS alone. We

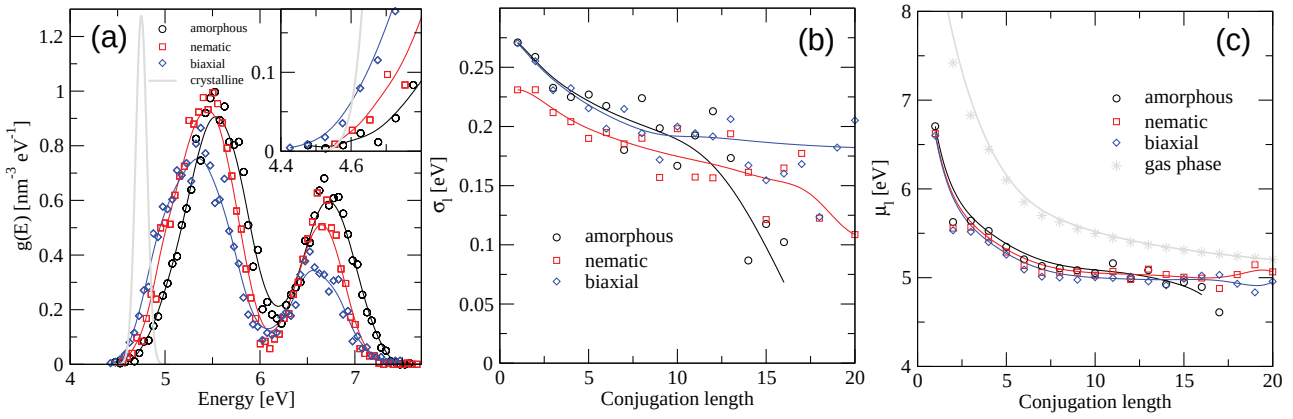

Figure 4. a) Hole density of states for the amorphous, nematic, and biaxial mesophase. With increasing structural order, the monomer peak decreases in favor of a developing low-IE shoulder around 5 eV. b) Conjugation-length resolved energetic disorder σ_l and c) energetic mean μ_l. Both σ_l and μ_l plateau as of conjugation lengths $l \gtrsim 6$. Note that the drop in σ_l observed in the amorphous and nematic system for large l is due purely to poor statistics.

note that the evolving shoulder at 5 eV (see also the inset) plays a crucial role for charge transport and highlights why in semicrystalline polymers amorphous regions will not easily participate in charge transport.[19]

It is furthermore instructive to consider the conjugation-length-resolved energetic disorder σ_1 and energetic mean $\mu_l = \langle \mathrm{IE} \rangle_l$, shown in Figure 4b,c, respectively. Indeed, both σ_l and μ_l plateau for conjugation lengths $l \gtrsim 6$. For σ_l , this behaviour is understood based on the correlation length of local (e.g., dipolar) fluctuations of the electric potential: Longer segments experience the averaged effect of these local perturbations, whereas short segments are subjected to the full effect of local disorder. For μ_l, the plateau results from the opposed action of increased delocalization (which reduces the internal IE) on the one hand and reduced inductive stabilization on the other hand. These length-compensating effects prove that the energy landscape is less sensitive to conjugation length than anticipated, provided an average conjugation length $l \gtrsim 6$. Interestingly, the mean of the DOS in crystalline P3HT in a face-on thin-film setup, studied via the same approach, is located at 4.75 eV and hence overlaps significantly with the DOS from Figure 4a. However, energetic disorder that accompanies paracrystallinity is significantly reduced in these crystalline regions, measuring only 0.06 eV, compared to 0.2 eV observed in the partially ordered phases (Figure 4b). It is hence expected that energetic disorder plays an even larger role than the energetic mean in setting apart the charge transport properties of ordered and partially ordered domains.

Finally, we turn to the spatial correlation function, which we define as an average over the correlation function of individual subpopulations of length l

$$C(R) = \left\langle \sum_l \frac{(\mathrm{IE}_{i(l)} - \mu_l)(\mathrm{IE}_{j(l)} - \mu_l)}{\sigma_l^2} \right\rangle_{r_{ij}=R} \quad (1)$$

C(R) is plotted for all three mesophases in Figure 3c. Indeed, the correlation function decays slower the more ordered the system, an effect that can be traced back to the increased long-range order that was inherited from the soft model. In biaxial systems, a weak spatial correlation of site energies already resulted from the spatial partitioning into ordered and less ordered regions.[23] Long-ranged electrostatics, however, significantly amplifies the effect of structural order on site-energy correlations.

3. Conclusions

To conclude, we have investigated the effect of partial order on the charge transport properties of polymeric semiconductors. To identify these effects systematically, we employed a sequence of mesophases with gradually increasing degree of molecular order—from completely amorphous via nematic uniaxial to biaxial liquid-crystalline. A three-step hierarchical scheme developed here proved capable of generating large-scale morphologies with atomistic detail, as required for the study of electronic properties: Initially morphologies are equilibrated on large scales using a recently developed soft model with anisotropic non-bonded interactions between particles representing entire repeat units. Subsequently the resolution is refined via an intermediate model derived from systematic coarse-graining that facilitates the insertion of all-atom details in the final step. We applied the procedure to P3HT as a test system and computed the energy landscape for holes in the resulting morphologies. We show that upon increasing structural order, low-energy states and spatial correlations amplify, with conjugation-length independent energetic disorder and energetic mean as of a moderate segment length of six repeat units. In comparison to crystalline systems, these findings indicate that the energy landscape of crystalline systems promotes efficient transport primarily because of the reduced energetic disorder that accompanies lamellar packing.

Supporting Information

Supporting Information is available from the Wiley Online Library or from the author.

Acknowledgements: This work was partially supported by the DFG program IRTG 1404, DFG grant SPP 1355, and BMBF grants MORPHEUS (FKZ 13N11704), MEDOS (FKZ 03EK3503B), and MESOMERIE (FKZ 13N10723). K.K. acknowledges research funding through the European Research Council under the European Unions Seventh Framework Programme (EP7/2007-2013)/ERC Grant Agreement No. 340906-MOLPROCOMP. Computing time at the MPG supercomputer hydra in Garching is gratefully acknowledged. The authors are grateful to Anton Melnyk for useful advice regarding the GROMACS package.

Received: December 17, 2014; Revised: January 24, 2015; Published online: March 10, 2015; DOI: 10.1002/marc.201400725

Keywords: charge transport; large-scale morphologies; multiscale simulations; P3HT

[1] R. Elsenbaumer, K. Jen, R. Oboodi, *Synthetic Metals* **1986**, *15*, 169.
[2] R. D. McCullough, R. D. Lowe, *Chem Comm.* **1992**, 70.
[3] J. Nelson, J. J. Kwiatkowski, J. Kirkpatrick, J. M. Frost, *Accounts Chem. Res.* **2009**, *42*, 1768.
[4] J. L. Brédas, D. Beljonne, V. Coropceanu, J. Cornil, *Chem. Rev.* **2004**, *104*, 4971.
[5] D. P. McMahon, D. L. Cheung, L. Goris, J. Dacuna, A. Salleo, A. Troisi, *J. Phys. Chem. C* **2011**, *115*, 19386.

[6] C. Poelking, M. Tietze, C. Elschner, S. Olthof, D. Hertel, B. Baumeier, F. Würthner, K. Meerholz, K. Leo, D. Andrienko, *Nat. Mater.* **2014**, DOI: 10.1038/nmat4167.
[7] P. Kordt, J. J. M. van der Holst, M. Al Helwi, W. Kowalsky, F. May, A. Badinski, C. Lennartz, D. Andrienko, *Adv. Funct. Mater.* **2015**, DOI: 10.1002/adfm.201403004.
[8] S. Few, J. M. Frost, J. Nelson, *Phys. Chem. Chem. Phys.* **2014**, *17*, 2311.
[9] O. Alexiadis, V. G. Mavrantzas, *Macromolecules* **2013**, *46*, 2450.
[10] C. Poelking, D. Andrienko, *Macromolecules* **2013**, *46*, 8941.
[11] C. Poelking, V. Ivanov, K. Kremer, C. Risko, J. L. Brédas, D. Andrienko, C. Eunkyung, *J. Phys. Chem. C* **2013**, *117*, 1633.
[12] D. M. Huang, R. Faller, K. Do, A. J. Moulé, *J. Chem. Theory Comput.* **2010**, *6*, 526.
[13] E. Jankowski, H. S. Marsh, A. Jayaraman, *Macromolecules* **2013**, *46*, 5775.
[14] K. N. Schwarz, T. W. Kee, D. M. Huang, *Nanoscale* **2013**, *5*, 2017.
[15] A. Lukyanov, A. Malafeev, V. Ivanov, H. L. Chen, K. Kremer, D. Andrienko, *J. Mater. Chem.* **2010**, *20*, 10475.
[16] V. Rühle, J. Kirkpatrick, D. Andrienko, *J. Chem. Phys.* **2010**, *132*, 134103.
[17] M. Müller, *J. Stat. Phys.* **2011**, *145*, 967.
[18] R. J. Kline, M. D. McGehee, E. N. Kadnikova, J. Liu, J. M. J. Fréchet, M. F. Toney, *Macromolecules* **2005**, *38*, 3312.
[19] R. Noriega, J. Rivnay, K. Vandewal, F. P. V. Koch, N. Stingelin, P. Smith, M. F. Toney, A. Salleo, *Nat. Mater.* **2013**, *12*, 1038.
[20] C. Poelking, K. Daoulas, A. Troisi, D. Andrienko, *P3HT Revisited – From Molecular Scale to Solar Cell Devices* (Ed: S. Ludwigs), Springer, Berlin, Heidelberg, Vol. no. 265, p. 139.
[21] A. M. Ballantyne, L. Chen, J. Dane, T. Hammant, F. M. Braun, M. Heeney, W. Duffy, I. McCulloch, D. D. C. Bradley, J. Nelson, *Adv. Funct. Mater.* **2008**, *18*, 2373.
[22] A. Zen, J. Pflaum, S. Hirschmann, W. Zhuang, F. Jaiser, U. Asawapirom, J. P. Rabe, U. Scherf, D. Neher, *Adv. Funct. Mater.* **2004**, *14*, 757.
[23] P. Gemünden, C. Poelking, K. Kremer, D. Andrienko, K. C. Daoulas, *Macromolecules* **2013**, *46*, 5762.
[24] R. L. Henderson, *Phys. Lett. A* **1974**, *49*, 197.
[25] A. Lyubartsev, A. Laaksonen, *Phys. Rev. E* **1995**, *52*, 3730.
[26] D. Reith, M. Pütz, F. Müller-Plathe, *J. Comput. Chem.* **2003**, *24*, 1624.
[27] B. Hess, C. Kutzner, D. van der Spoel, E. Lindahl, *J. Chem. Theory Comput.* **2008**, *4*, 435.
[28] V. Rühle, C. Junghans, A. Lukyanov, K. Kremer, D. Andrienko, *J. Chem. Theory Comput.* **2009**, *5*, 3211.
[29] T. J. Prosa, M. J. Winokur, J. Moulton, P. Smith, A. J. Heeger, *Macromolecules* **1992**, *25*, 4364.
[30] M. Bouhassoune, S. van Mensfoort, P. Bobbert, R. Coehoorn, *Org. Electron.* **2009**, *10*, 437.
[31] R. Coehoorn, W. F. Pasveer, P. A. Bobbert, M. A. J. Michels, *Phys. Rev. B* **2005**, *72*, 155206.
[32] H. Baessler, *Phys. Status Solidi B* **1993**, *175*, 15.
[33] P. Prins, F. C. Grozema, L. D. A. Siebbeles, *Mol. Simul.* **2006**, *32*, 695.
[34] J. Rivnay, R. Noriega, J. E. Northrup, R. J. Kline, M. F. Toney, A. Salleo, *Phys. Rev. B* **2011**, *83*, 121306.
[35] J. M. Frost, J. Kirkpatrick, T. Kirchartz, J. Nelson, *Faraday Discuss.* **2014**, *174*, 255.
[36] H. Ma, T. Qin, A. Troisi, *J. Chem. Theory. Comput.* **2014**, *10*, 1272.
[37] D. P. McMahon, A. Troisi, *Chem. Phys. Lett.* **2009**, *480*, 210.
[38] N. Vukmirović, L. W. Wang, *J. Phys. Chem. B* **2009**, *113*, 409.
[39] N. Vukmirović, L. W. Wang, *Nano Lett.* **2009**, *9*, 3996.
[40] N. Vukmirović, L. W. Wang, *J. Phys. Chem. B* **2011**, *115*, 1792.
[41] D. Porezag, T. Frauenheim, T. Köhler, G. Seifert, R. Kaschner, *Phys. Rev. B* **1995**, *51*, 12947.
[42] M. Elstner, D. Porezag, G. Jungnickel, J. Elsner, M. Haugk, T. Frauenheim, S. Suhai, G. Seifert, *Phys. Rev. B* **1998**, *58*, 7260.
[43] Å. Johansson, S. Stafström, *Phys. Rev. Lett.* **2001**, *86*, 3602.
[44] W. Barford, D. Trembath, *Phys. Rev. B* **2009**, *80*, 165418.
[45] V. Rühle, A. Lukyanov, F. May, M. Schrader, T. Vehoff, J. Kirkpatrick, B. Baumeier, D. Andrienko, *J. Chem. Theory. Comput.* **2011**, *7*, 3335.